Hindawi
International Journal of Aerospace Engineering
Volume 2018, Article ID 7021038, 15 pages
https://doi.org/10.1155/2018/7021038

Research Article

An Improved Fuzzy Neural Network Compound Control Scheme for Inertially Stabilized Platform for Aerial Remote Sensing Applications

Xiangyang Zhou,[1,2] **Yating Li**,[1] **Yuan Jia**,[3] **and Libo Zhao**[2]

[1]*School of Instrumentation Science & Opto-Electronics Engineering, Beihang University, Beijing 100191, China*
[2]*State Key Laboratory for Manufacturing Systems Engineering, Xi'an Jiaotong University, Xi'an 710049, China*
[3]*China Aerospace Academy of Electronic Technology Beijing Institute of Aerospace Micro-Electromechanical Technology, Beijing 100094, China*

Correspondence should be addressed to Xiangyang Zhou; xyzhou@buaa.edu.cn and Libo Zhao; libozhao@mail.xjtu.edu.cn

Received 28 February 2018; Accepted 30 June 2018; Published 1 August 2018

Academic Editor: Kenneth M. Sobel

An improved fuzzy neural network (FNN)/proportion integration differentiation (PID) compound control scheme based on variable universe and back-propagation (BP) algorithms is proposed to improve the ability of disturbance rejection of a three-axis inertially stabilized platform (ISP) for aerial remote sensing applications. In the design of improved FNN/PID compound controller, the variable universe method is firstly used for the design of the fuzzy/PID compound controller; then, the BP algorithm is utilized to finely tune the controller parameters online. In this way, the desired performances with good ability of disturbance rejection and high stabilization accuracy are obtained for the aerial ISP. The simulations and experiments are, respectively, carried out to validate the improved FNN/PID compound control method. The results show that the improved FNN/PID compound control scheme has the excellent capability in disturbance rejection, by which the ISP's stabilization accuracy under dynamic disturbance is improved significantly.

1. Introduction

For a high-resolution aerial remote sensing system, it needs the inertially stabilized platform (ISP) to isolate the attitude changes of an aircraft in the directions of three axes and to reject the multisource disturbances in real time whether they are inside or outside of the aircraft body; therefore, the ISP is a key component for an aerial remote sensing system, which is mainly used to hold and control the line of sight (LOS) of the imaging sensors keeping steady in the inertial space [1–5]. The first fundamental objective of an ISP is to help imaging sensors to obtain high-resolution images of the target. Therefore, the most critical performance metric for an ISP is the disturbance rejection.

Disturbances that affect the pointing vector arise from platform angular motion or maneuvers and external loads such as wind and airstream inducing torque. Disturbances arise from diverse sources; for example, the linear motion and vibration of the aircraft platform generate disturbance torques due to mass imbalance and gimbal geometry. Among these disturbances, friction, imbalance, vehicle motion kinematic coupling, and sensor noise are predominant [6, 7]. It is a principal issue for the control system of the ISP to minimize the effects of disturbances on the ISP. In [5], a compound scheme on parameter identification and adaptive compensation of nonlinear friction disturbance is proposed to improve the stabilization accuracy of the ISP. In [6], a dual-rate-loop control method based on a disturbance observer (DOB) of angular acceleration is proposed to improve the control accuracy and stabilization of the ISP. In [7], the common disturbances in the ISP are summarized systematically. In [8], a composite control method based on the adaptive radial basis function neural network (NN) feedback control and the extended state observer is applied to a

two-axis ISP system. In [9], an adaptive decoupling control for three-axis gyro stabilized platform based on the NN is proposed. In [10], a three-closed-loop compound controller for a two-axis ISP with multisensors is proposed and validated by experiments. The best-known application of ISPs is stabilization and control of payloads such as electro-optical sensors and laser beams [11]. In [12], to realize a balance between high performance and complexity, a dual-stage inertial stabilization system based on frequency-domain analysis is established. In [13, 14], a high-precision control scheme based on active disturbance rejection control (ADRC) and a model reference adaptive control (MRAC)/PID command scheme are, respectively, proposed for the disturbance rejection of the ISP.

Compared with other methods, the fuzzy control is an adaptive approach of intelligent control, which can deal with the nonlinear, complex, and sometimes mathematically intangible dynamic systems. It has been applied for a wide range [15–22]. It provides a convenient method for constructing nonlinear controllers via the use of heuristic information [23, 24]. The fuzzy control can ensure that the system maintains a small overshoot with fast response, which has a strong adapted ability to the change of control parameters. For the nonlinearity or complexity of the control object, it has the advantages of good robustness and strong anti-interference ability. Since it is not necessary to establish the mathematical model of the controlled object, therefore, it is very suitable for improving the immunity and stability of the ISP. However, there is an inevitable steady-state error when the fuzzy control is used in a control process. So, the fuzzy control and other control methods need to be used in combination so as to achieve a high stabilization accuracy control. Among these methods, the PID controller takes the error as an input, which can satisfy the different requirements of the PID parameter self-tuning [25]. Therefore, if the fuzzy and the PID control methods were combined to establish a fuzzy/PID compound controller, the PID parameters can be adjusted in real time on the basis of the fuzzy controller. Thus, the dynamic performance and disturbance rejection ability of the ISP control system can be improved.

In general, the fuzzy/PID compound controller is experimentally designed based on the fixed universes. In order to improve the control accuracy, the number of fuzzy partitions should be increased. But the increase in the number of fuzzy subsets will lead to the so-called rule explosion problem which makes the controller design difficult. The variable universe can make use of the contraction-expansion factors to achieve the equivalent results resembling the increase in the number of fuzzy subsets [26]. Since there is no typical generalization capability, the design of the variable universe fuzzy/PID compound controller is relying on the experts' knowledge and experience so that more parameters need to be adjusted further [27]. With the universal approximation ability, the neural network (NN) has become a powerful approximation tool for system control, which generates their own rules by learning [28]. The stabilization of a gimbal platform for optical sensor acquisitions in topographic applications using mobile vehicles is investigated, and an NN-based approach was developed to stabilize the gimbal platform [29]. Since the NN is able to deliver highly desired learning faculties while the fuzzy/PID compound controller just lacks this capability, it could provide a highly desired functional skeleton for the fuzzy/PID compound controller [30]. In addition, due to the self-learning ability, the back-propagation (BP) algorithm can fine-tune the weight coefficient value of the system, as well as reducing the dependence of the controller performance on the initial value of the parameters and the tracking error under the interference. In [31], an improved BP neural network algorithm to detect anomaly network traffic with adjusted correlation rules is developed.

In this paper, an improved FNN/PID compound control scheme is proposed to improve the ability of disturbance rejection and the stabilization accuracy of an aerial ISP. In the scheme, the variable universe method is used for the design of the fuzzy/PID compound controller to improve the convergence at an early period, and the BP algorithm is used to fine-tune the controller parameters online. To verify the scheme, the simulations and experiments are carried out, respectively. Compared to our previous publications [13, 14], the novel and significant contribution of this paper is to propose an improved FNN/PID compound control scheme, in which the idea of variable universe and the BP algorithm are combined to improve the ability of disturbance rejection.

2. Background

2.1. Aerial Remote Sensing System. Figure 1 shows the schematic diagram of an aerial remote sensing system. Generally, an aerial remote sensing system consists of four main components, a three-axis ISP, a remote sensing sensor, a position and orientation system (POS), and an aviation platform. When the aviation platform rotates or jitters, the control system of the ISP gets the high-accuracy attitude reference information measured by the POS and then routinely controls the LOS of the imaging sensor to achieve accurate pointing relative to ground level and flight track [13, 14].

The function of the ISP is to act as an intelligent and physical interface between the remote sensing sensor and the aircraft. With the help of ISP, the influences of various disturbances either inside or outside the aircraft on the remote sensing sensor are initiatively isolated, hence leading to high-resolution images. The POS, which is mainly composed of three main components, inertial measurement unit (IMU), GPS receiving antenna, and data processing system [32], is used to provide an accurate reference of position and attitude in the inertial space for the control system of the ISP and imaging sensor through measuring the angular movement of the imaging sensor. The IMU is mounted on the top of the imaging sensor phase center [5].

2.2. Operating Principle of the Three-Axis ISP System. Figure 2 shows the schematic diagram of the three-axis ISP. We can see that the ISP consists of three gimbals, which are azimuth gimbal, pitch gimbal, and roll gimbal, respectively. G_x, G_y, and G_z, respectively, stand for the rate gyro that measures the inertial angular rate of the three gimbals.

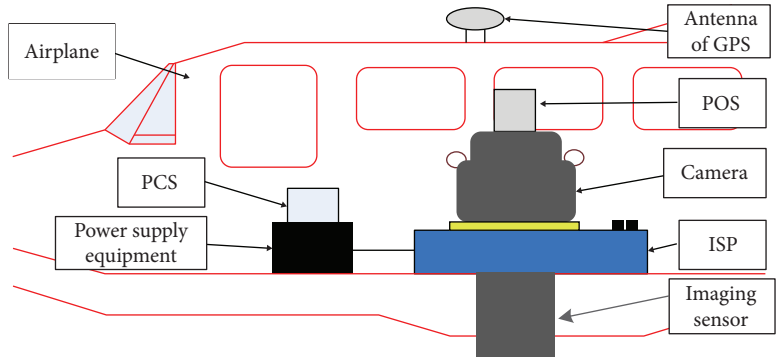

Figure 1: Schematic diagram of an aerial remote sensing system.

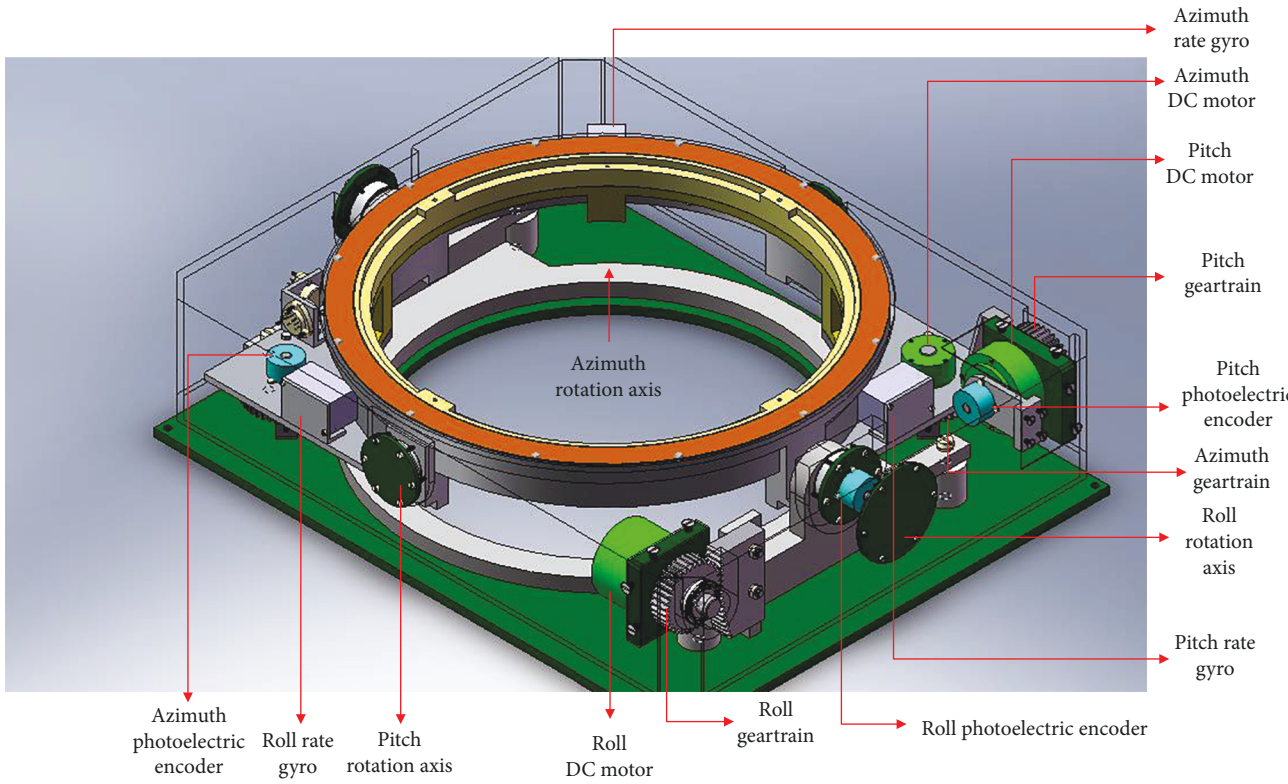

Figure 2: Schematic diagram of the three-axis ISP.

E_x, E_y, and E_z, respectively, stand for the photoelectric encoder which measures the relative angular rate between gimbals. M_r, M_p, and M_a, respectively, stand for the gimbal servo motor of the three gimbals [13, 14].

2.3. Three-Closed-Loop Compound Controller. Figure 3 shows the block diagram of a traditional three-loop control system for the ISP [13, 14]. *G*-pos, *G*-spe, and *G*-cur separately represent the controllers in the tracking loop, stabilization loop, and current loop. PWM represents the power amplification used to amplify the current to drive the torque motor. *L* represents the inductance of the torque motor, and *R* represents the resistance. k_T represents the torque coefficient of the motor, and *N* is the transition ratio from the torque motor to the gimbals. J_m represents the moment of inertia of the motor, and J_l represents the moment of inertia of the gimbals along the rotation axis.

For all of the three gimbals, the control systems are the same three-loop compound control structure, as shown in Figure 3. The specific functions of the three loops can be summarized as follows: the inner current loop is used to reduce the influence of voltage fluctuation from power supply or motor back electromotive force; the middle stabilization loop uses a rate gyro to measure the angular rate of each gimbal in the inertial space, which is used to compensate the difference between the rate command input and the angular rate of the gimbal and then improve the steady-

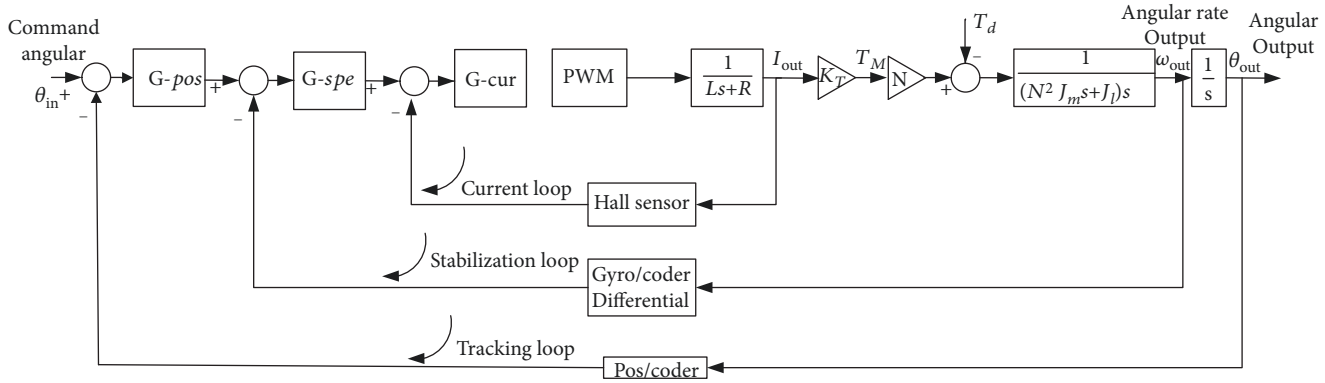

Figure 3: A block diagram of a traditional three-loop control system for the ISP.

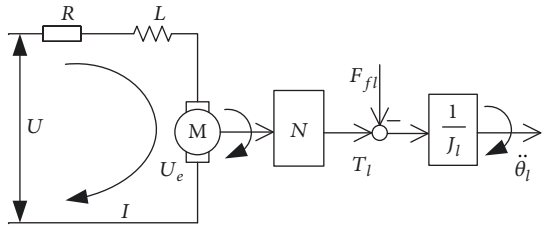

Figure 4: Block diagram for a simplified gear drive system with fixed transmission ratio.

state precision; and as to the main feedback path, the outer tracking loop takes the attitude angle measured by POS as accurate references to ensure the accurate pointing of the LOS [5].

To realize the high-drive torque of the load under the limitation of small size, the motor and gear train with high transmission ratio are usually used in the design of ISPs. If the influence of the backlash is ignored, the system model can be simplified with fixed transmission ratio, as shown in Figure 4 [5].

According to the current balance equation and the torque balance equation, at the side of the motor output axis, the following equations are satisfied:

$$\begin{aligned} U &= IR + L\frac{dI}{dt} + k_b\omega_m, \\ J_m\ddot{\theta}_m + b_m\omega_m &= T_m - \tau_l - F_{fm}, \\ T_m &= k_T I, \end{aligned} \tag{1}$$

where U, I, R, and L are the armature voltage, current, resistance, and inductance of the torque motor, respectively; k_b is the back EMF constant of the motor; ω_m is the angular velocity of the motor; J_m is the rotational inertia of the motor; θ_m is the angular displacement of the motor; b_m is the equivalent damping of the motor; T_m is the electromagnetic torque of the motor; τ_l is the load torque at the side of the motor output axis; F_{fm} is the inner friction torque of the motor; and k_T is the torque coefficient of the motor.

3. Design of the Improved FNN/PID Compound Controller

In the design of the improved FNN/PID compound controller, firstly, the variable universe method is used for the design of the fuzzy/PID compound controller, and then, the BP algorithm is used to fine tune the controller parameters online to improve the performance of the FNN/PID compound controller.

3.1. Fuzzy/PID Compound Controller Based on Variable Universe. Figure 5 shows the structure of the fuzzy/PID compound controller. In this work, the fuzzy/PID compound controller makes use of the nonlinear mapping of applied fuzzy logic to establish the angle position error parameters e and ec, as well as three PID parameters. On the basis of the input change, it adjusts the control gain in real time so as to obtain the fast-response ability to large deviation and the fine adjustment to small deviation. The combination of the parameters based on the fuzzy logic and the PID initial value is as follows:

$$\begin{aligned} K_p &= K_{p0} + \text{Fuzzy}(\Delta K_p), \\ K_i &= K_{i0} + \text{Fuzzy}(\Delta K_i), \\ K_d &= K_{d0} + \text{Fuzzy}(\Delta K_d), \end{aligned} \tag{2}$$

where K_{p0}, K_{i0}, and K_{d0} represent the initial parameters of the fuzzy/PID compound controller.

Fuzzification is an accurate numerical classification, which sets a fuzzy set corresponding to each file. The subsets of fuzzy languages are selected as negative big, negative middle, negative small, zero, positive small, positive middle, and positive big and also expressed as {NB, NM, NS, ZE, PS, PM, PB}, respectively [33]. The input universes are taken as $\{-6, -5, -4, -3, -2, -1, 0, 1, 2, 3, 4, 5, 6\}$. Based on simulation analysis, the membership function of nonlinear distribution is finally used [34].

Under the normal circumstances, a combination of the fuzzy control and PID control in the ISP relies on increasing the fuzzy rules to obtain higher accuracy, but it easily leads to the regular explosion. Therefore, the variable universe method is introduced in the controller design, which can

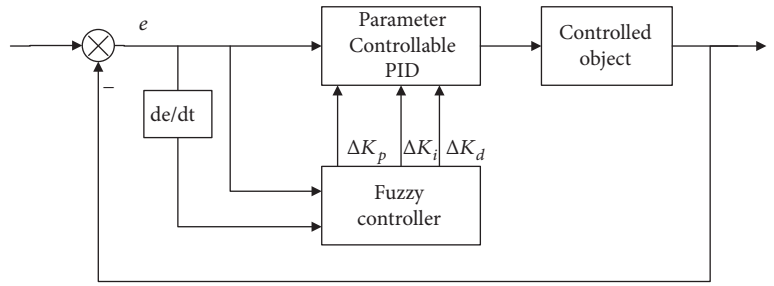

Figure 5: Fuzzy/PID compound controller structure.

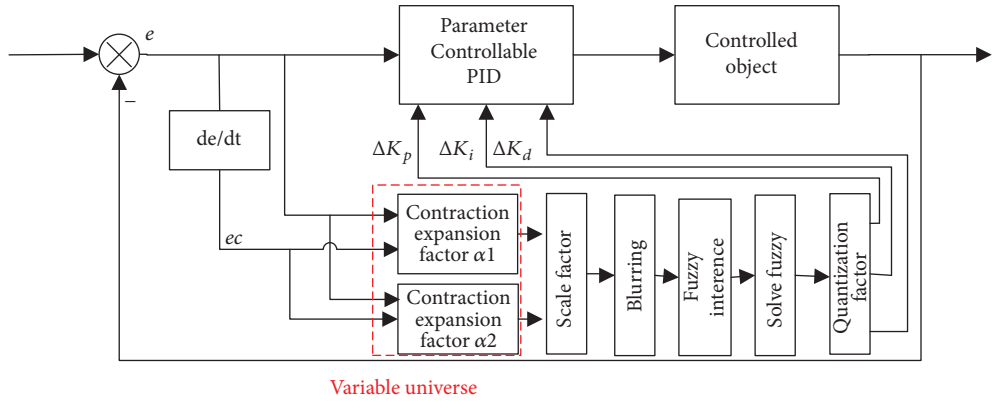

Figure 6: Variable universe fuzzy/PID compound controller structure.

improve the control effect under the same number of rules. In particular, the method is to introduce the contraction expansion factors, α_1 and α_2, on the basis of the fuzzy/PID compound controller, so that the universe of e and ec is $\{-U_1{}^*\alpha_1, U_1{}^*\alpha_1\}$ and $\{-U_2{}^*\alpha_2, U_2{}^*\alpha_2\}$, respectively. Thus, the corresponding output amounts can change according to different contraction expansion factors. In the experiments, the contraction expansion factors, α_1 and α_2, are chosen optimally as 0.25 and 0.5, respectively, so that the controller can converge quickly and have small stabilization error. Figure 6 shows the diagram of the variable universe fuzzy/PID compound controller.

3.2. FNN/PID Compound Control Scheme. The fuzzy control and the NN are frequently combined in a compound scheme called the FNN [35, 36]. The general FNN-combined PID controller is composed of two parts: the PID/NN and the FNN, which are the front part and the latter part of the controller, respectively. Through the learning offline and online, the real-time adaptive capability of the NN is trained so that the part of the fuzzy logic can be adjusted.

In the FNN using the second-order method, the fuzzy layers follow the two input nodes of the first layer. The two input nodes of the first layer are named as the deviation and the deviation rate, that is, e and ec, respectively. Since the number of nodes in the fuzzy layer depends on the number of fuzzy subsets divided by e and ec, the membership function, which is the activation function in the network, can be written by using the Gaussian functions:

$$\mu_{Aij} = \exp\left[\frac{-(X_i - c)^2}{\sigma^2}\right], \tag{3}$$

where X_i, c, and σ represent the input variable, the activation function center, and the activation function width, respectively. The subscript A represents the fuzzy subset of the fuzzy variable. The number of nodes in the fuzzy rule layer is the number of fuzzy rules, which is shown as follows:

$$O_k = \mu_{A1k}(x_1) * \mu_{A2k}(x_2), \tag{4}$$

where O_k represents the degree of activation about the rule k. The weighted average method is usually used in the defuzzy layer. The front structure of the FNN is shown in Figure 7.

The input and output relationship of each node is shown in the following formula. The first-layer input (input layer) is

$$I_i^{(1)} = X_i, \quad i = 1, 2. \tag{5}$$

The first-layer output is

$$O_i^{(1)} = I_i^{(1)}, \quad i = 1, 2. \tag{6}$$

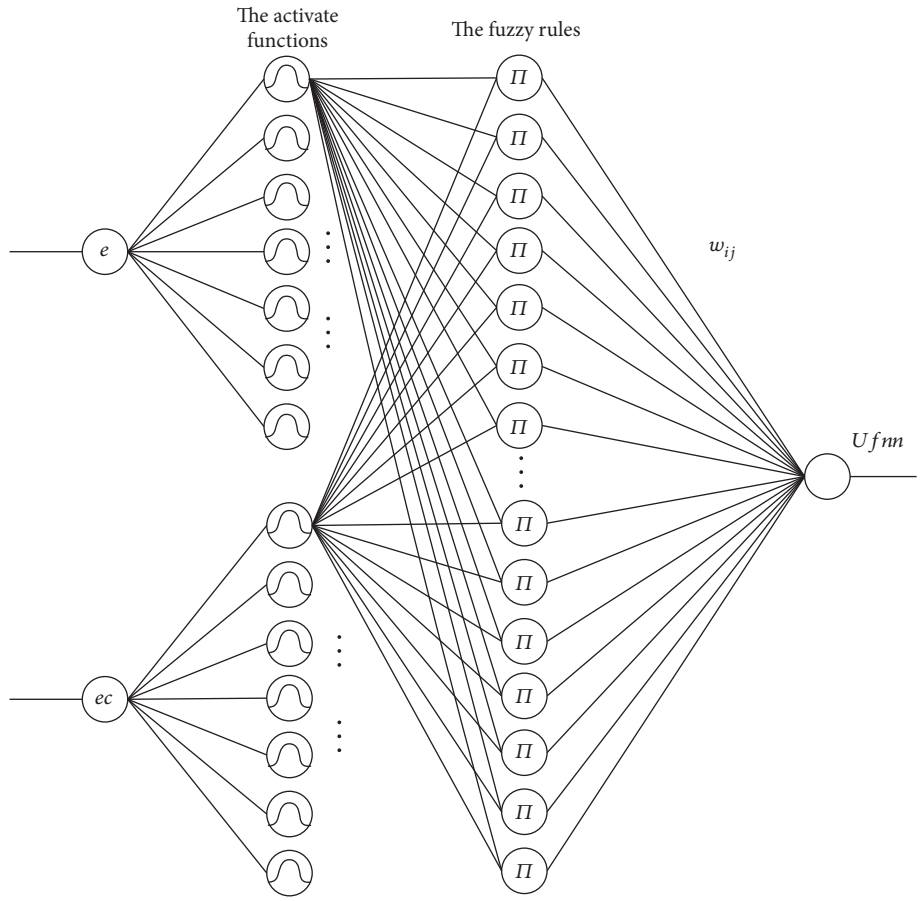

Figure 7: The front topological structure of the FNN.

The second-layer input (fuzzy layer) is

$$I_{ij}^{(2)} = \frac{-\left(O_{ij}^{(1)} - c\right)^2}{\sigma^2}, \quad i = 1, 2, j = 1, 2, \ldots, n. \tag{7}$$

The second-layer output is

$$O_{ij}^{(2)} = \exp\left(I_{ij}^{(2)}\right), \quad i = 1, 2, j = 1, 2, \ldots, n. \tag{8}$$

The third-layer input (fuzzy rule layer) is

$$I_{(j-1)n+k}^{(3)} = O_{1j}^{(2)} O_{2k}^{(2)}, \quad j = 1, 2, \ldots, n, k = 1, 2, \ldots, n. \tag{9}$$

The third-layer output is

$$O_i^{(3)} = I_i^{(3)}, \quad i = 1, 2, \ldots, n^2. \tag{10}$$

The fourth-layer input (defuzzy layer) is

$$I^{(4)} = \sum_{i=1}^{n^2} O_i^{(3)} wf_i, \tag{11}$$

where wf_i is the connected weight of the output layer.

The output of the fourth layer is

$$O_i^{(4)} = \frac{I^{(4)}}{\sum_{i=1}^{n^2} O_i^{(3)}}, \tag{12}$$

where n is the number of fuzzy subsets about the deviation and the deviation change rate.

The deviation e and deviation change rate ec are taken as the input of the fuzzy controller, adjusting the PID parameters K_p, K_i, and K_d, according to fuzzy control rules, to reduce the impact of control model time variation [37]. On the basis of the FNN, the introduction of neurons of P, I, and D makes the network become a dynamic network, which can enhance the information processing ability of the network and can reflect the dynamic behaviour of the system better. The PID topological structure of the FNN is shown in Figure 8.

The NN is introduced into the fuzzy control to achieve the adaptive adjustment of fuzzy rules, by which the NN structure is used to complete the fuzzy system function, including the extraction and the adjustment of the rule. Since the output of the front part network is the same as the input of the back part, in which the indirect control parameters (the nonlinear mapping of error and error change) are

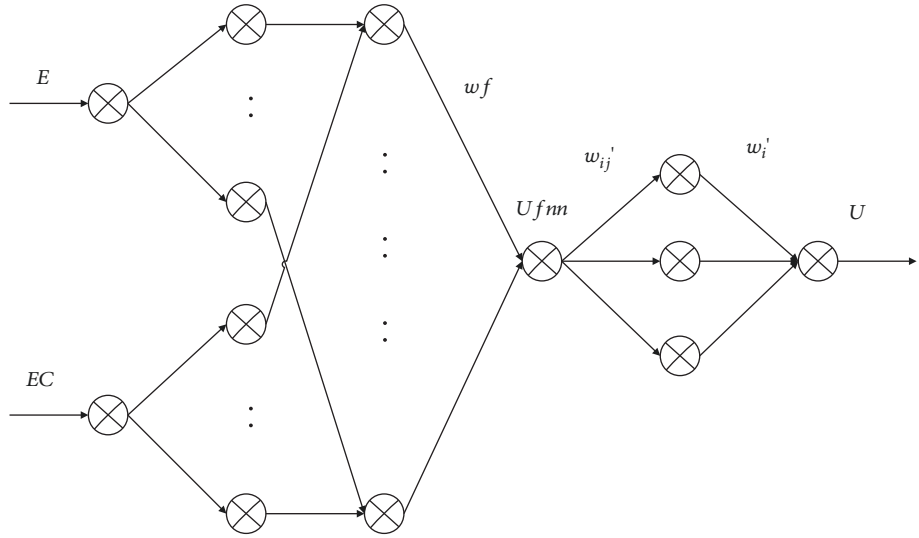

Figure 8: The PID topological structure of the FNN.

weighted and then input to the hidden layer of the back part network, the neurons of the hidden layer produce the PID control effect on the system. In this way, the control parameters are improved in real time, which integrate the advantages of the fuzzy, the NN, and the PID.

By using the incremental PID control algorithm, the output formula of the controller is derived as follows:

$$U(k) = \mathbf{w}_1'\mathbf{w}_{11}'U_{\text{fnn}}(k) + \mathbf{w}_2'\mathbf{w}_{21}'[U_{\text{fnn}}(k) + U_{\text{fnn}}(k-1)] + \mathbf{w}_3'\mathbf{w}_{31}'[U_{\text{fnn}}(k) - U_{\text{fnn}}(k-1)], \tag{13}$$

where U is the final output of the network, which is the system controlled variable; $\mathbf{w}_i'$ is the weight coefficient matrix about the PID layer and output layer; $\mathbf{w}_{ij}'$ is the weight coefficient matrix about the PID layer and input layer; and U_{fnn} is the output of the FNN, which is actually a nonlinear mapping of error.

The main control principle of the FNN/PID compound control scheme is that on the basis of the error and error changes of the input, the controller learning algorithm can adjust and update their weight constantly, which output a more suitable control amount for the current state of the system so that the output of the system is closer to the desired input [38].

3.3. BP Algorithm Fine-Tuning Online. After obtaining the offline suboptimal controller parameters, the BP algorithm is used to adjust the online simulations. The BP algorithm is adjusted on the basis of the initial parameters; therefore, the result of the offline acquisition is more close to the optimal value; it can more avoid the divergence or convergence to the suboptimal solution, but not the convergence to the optimal solution. Hence, only by offline, get better initial suboptimal parameters in order to better real-time online adjustment. The online BP algorithm adjustment is adjusted according to the following formula:

$$\begin{aligned} c(n+1) &= \frac{(c(n) + \text{xite}^* \partial E)}{(\partial c + \eta^* \Delta c(n))}, \\ \sigma(n+1) &= \frac{(\sigma(n) + \text{xite}^* \partial E)}{(\partial \sigma + \eta^* \Delta \sigma(n))}, \\ w_{\text{all}}(n+1) &= \frac{(w_{\text{all}}(n) + \text{xite}^* \partial E)}{(\partial w_{\text{all}} + \eta^* \Delta w_{\text{all}}(n))}, \end{aligned} \tag{14}$$

where w_{all} contains all the weights that need to be adjusted in the controller, xite represents the learning factor, and η is the momentum factor. E is the mean square error (MSE), which is expressed as $E = (1/2)(\text{rin}(k)\text{-yout}(k))^2$.

3.4. Improved FNN/PID Compound Control Scheme. For the existing FNN/PID compound control scheme, the initial parameter value has a great effect on the controller convergence. Since there are so many parameters, it is hard to find good initial values to realize the good control effects.

Combined with the fuzzy/PID, the FNN/PID has the advantages of small initial value dependency and easy convergence; besides, it also inherits the adaptive characteristics of the NN by the FNN/PID; the good control parameters can be obtained, such as high accuracy, small overshoot, and fast response speed.

In the improved FNN/PID controller, the input layer is composed of two nodes, *e* and *ec*, respectively. And the role of the fuzzy layer is designed to deal with the higher input and then start reasonable fuzzy segmentation; the number of nodes is equal to the number of subsets of variables.

$$f_1(i) = X = [x_1, \ldots, x_n], \quad n = 2. \tag{15}$$

When the improved FNN/PID compound control scheme is applied to the ISP, the accuracy should be taken into account; the fuzzy languages of each input variable are

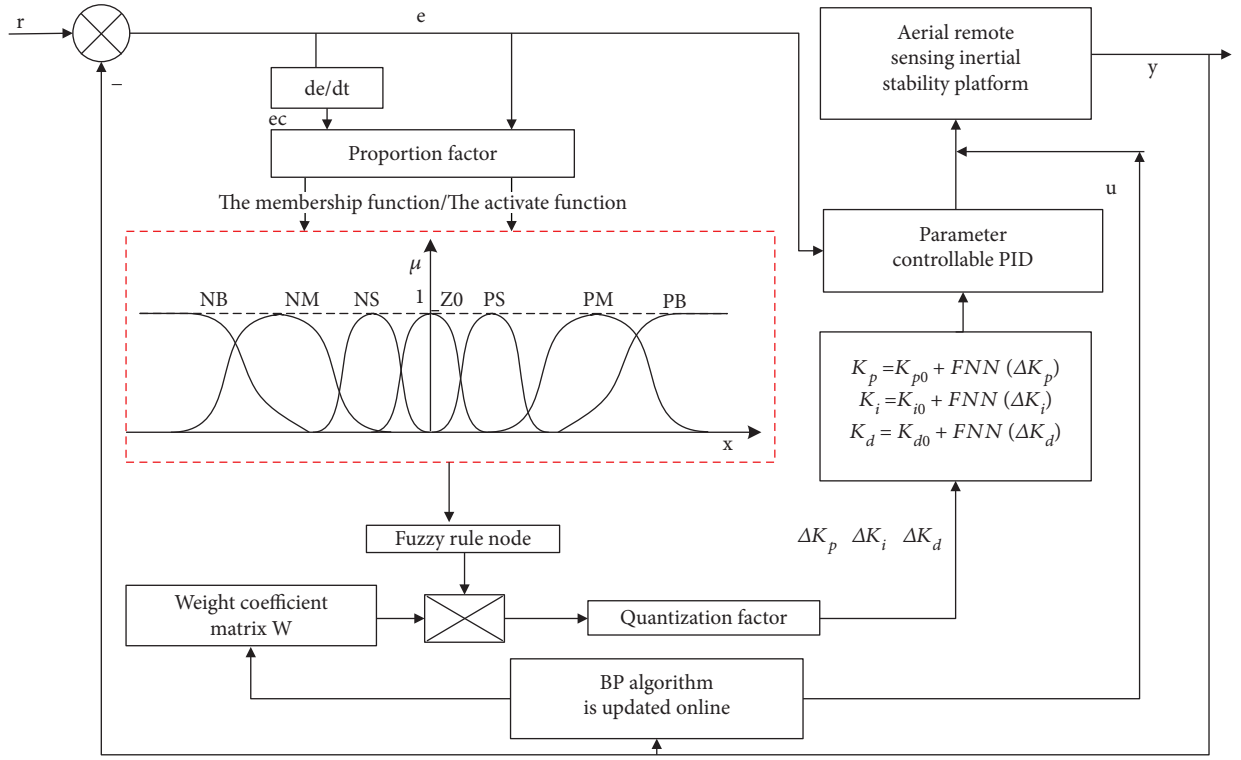

Figure 9: Schematic diagram of an improved FNN/PID compound control structure.

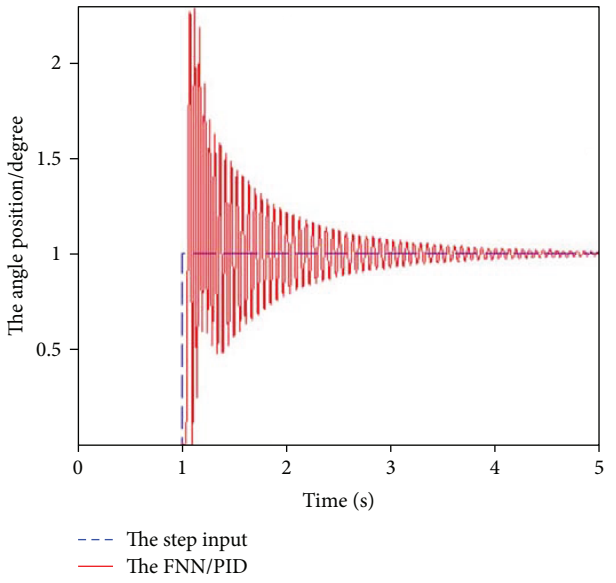

Figure 10: The response diagram of the FNN/PID controller under the step input.

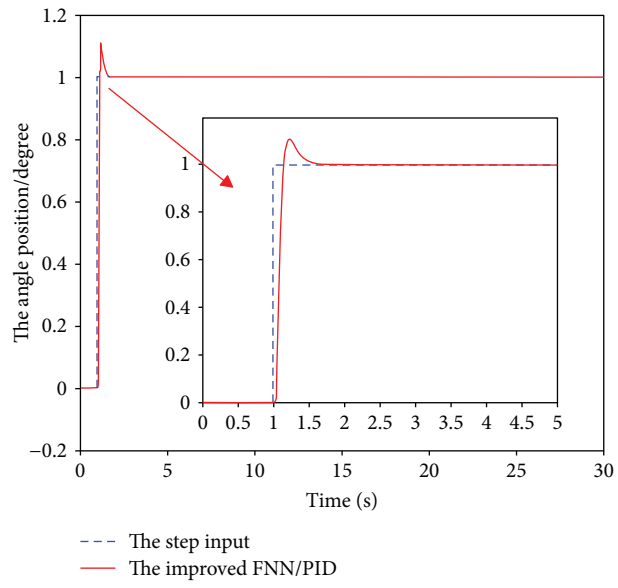

Figure 11: System response curve between the improved FNN/PID compound control scheme and step input.

Table 1: The accuracy of the FNN/PID compound control scheme in different time periods.

Time range (s)	0–30	5–10	3–30
RMS error (°)	0.0857	0.0015	0.0066

Table 2: Comparison of the accuracy of each method step response in different time periods.

Method	0–30 s/RMS error (°)
PID	0.0931
Fuzzy/PID	0.0770
Improved FNN/PID	0.0432

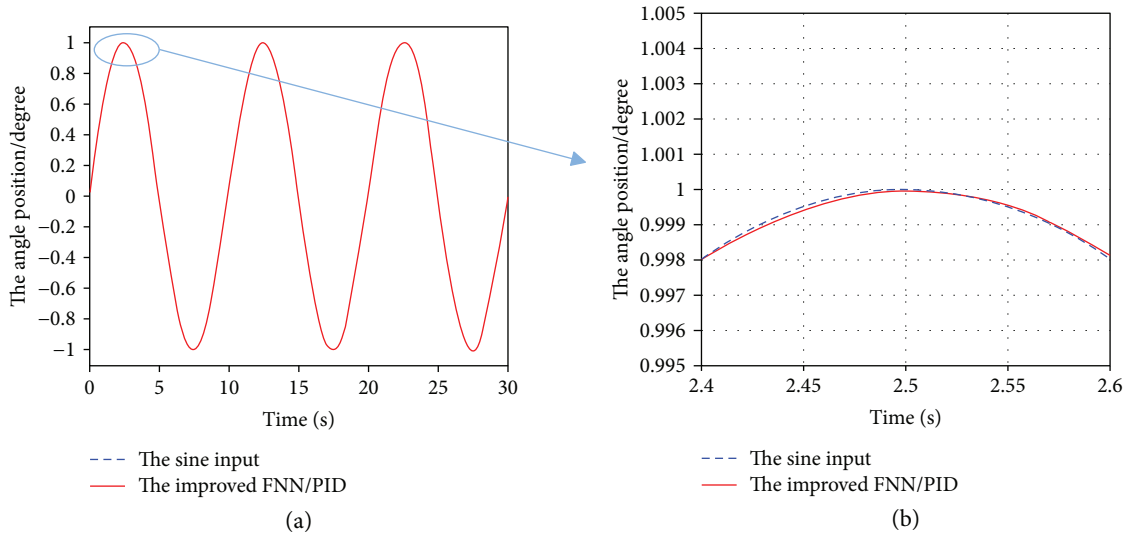

Figure 12: The sine response curve under the friction disturbance: (a) improved FNN/PID compound control schemes and (b) the partial enlargement.

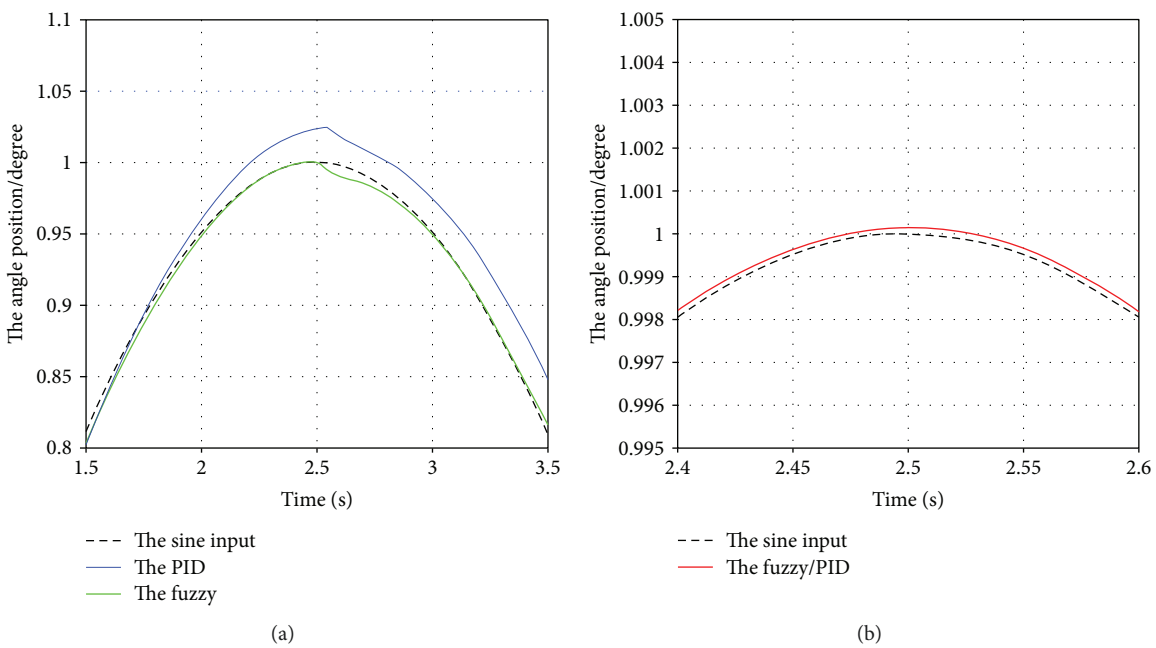

Figure 13: The comparison of system responses to sine input among different methods under the friction disturbance: (a) PID and fuzzy controller and (b) fuzzy/PID compound controller.

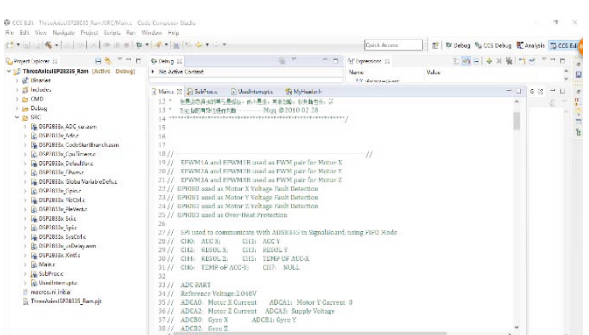

Figure 14: The control software.

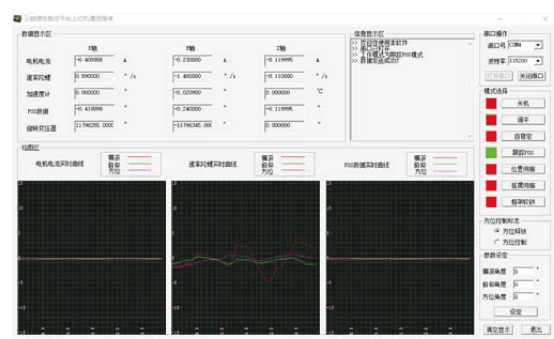

Figure 15: The upper computer software.

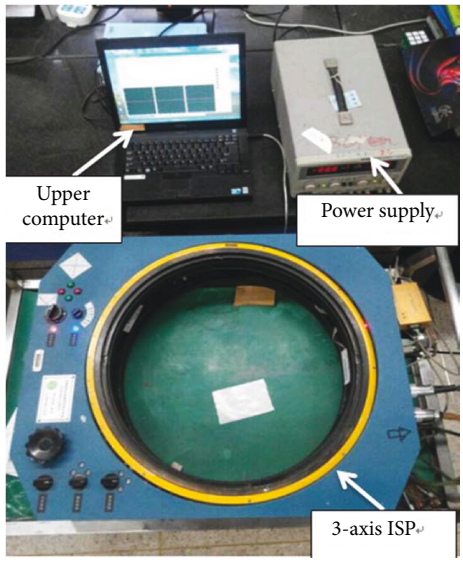

Figure 16: The picture of the three-axis ISP system in levelling static experiments.

divided into seven segments. According to the working principle of the ISP, in different fuzzy subsets, use different Gaussian functions and bell functions to represent.

$$f_2(i,j) = \mu_{Aij} = \exp\left[\frac{-(X_i - c_{ij})^2}{\sigma_{ij}^2}\right], \quad i = 1,2, j = 2,3,4,5,6,$$
$$f_2(i,j) = \mu_{Aij} = \frac{1}{\left(1 + \left|X_i - c_{ij}\right)/a_{ij}\right|)^{2\sigma_{ij}^2}}, \quad i = 1,2, j = 1,7. \tag{16}$$

Different from the simple activation function that is set by the general FNN/PID control algorithm, the parameters of the membership function about the improved method are different, which gain the experience about the fuzzy/PID compound controller from the membership function design. Therefore, it is more suitable for the system characteristics of the ISP. Since its parameters are no longer updated in the BP algorithm in real time, the blindness during the parameter updating is avoided and the calculation resources are saved, which is helpful to improve the control effect.

Correspondingly, the fuzzy rule layer has 49 nodes, and the fuzzy reasoning is calculated as

$$f_3(j) = \prod_{j=1}^{N} f_2(i,j) = \mu_{A1k}(x_1) * \mu_{A2k}(x_2), \quad N = \prod_{i=1}^{n} N_i. \tag{17}$$

For the output layer, omit the steps of the weighted average method and multiply the output of the upper layer directly by the connection weight matrix; the formula is shown as

$$f_4(j) = w \cdot f_3 = \sum_{j=1}^{N} w(i,j) \cdot f_3(j). \tag{18}$$

The output of the improved FNN/PID compound control scheme is taken as the compensation of the constant PID parameters:

$$\begin{aligned} K_p &= K_{p0} + \mathrm{FNN}(\Delta K_p), \\ K_i &= K_{i0} + \mathrm{FNN}(\Delta K_i), \\ K_d &= K_{d0} + \mathrm{FNN}(\Delta K_d). \end{aligned} \tag{19}$$

So, the output formula of the controller is

$$u(k) = k_p[e(k) - e(k-1)] + k_i \sum_{i=1}^{k} e(i) + k_d[e(k) - e(k-1)]. \tag{20}$$

In the improved FNN/PID compound control scheme, the FNN only computes a small amount of change and reduces the dependency on the initial value, so the adjustment time becomes shorter. The control of the entire system has good stability as it is not entirely dependent on the output of the adaptive adjustment part. The improved FNN/PID compound control scheme structure is shown in Figure 9.

In the improved FNN/PID compound control scheme, since the number of fuzzy subsets, the membership function, the quantization factor, and constant PID parameters are used, therefore, it needs only to determine the weight of the controller. Since the output of the method is small, the effect of the initial value of the weight coefficient on its output is limited.

4. Simulations Analysis

To analyse the performance of the proposed methods, the simulations are conducted under the MATLAB/Simulink software environment. It should be noted that in both simulations and experiments of this work, since the influences of the interactions between gimbals are very small compared to other disturbances [39], they are ignored when simulations and experiments are conducted.

The LuGre friction model described by (21) is added into the PID model to exhibit the effects of nonlinear friction disturbances on the performance of the control system. Also, to show the effects of the proposed FNN/PID compound controller on nonlinear disturbance rejection, the LuGre friction model is also added into the FNN/PID controller to exhibit its disturbance rejection ability.

The LuGre friction model of the ISP can be established as follows [5]:

$$\begin{aligned} \frac{dz}{dt} &= \omega_f - \frac{|\omega_f|}{g(\omega_f)} z, \\ \sigma_0 g(\omega_f) &= T_c + (T_s - T_c) e^{-(\omega_f/\omega_s)^2}, \\ F_{fl} &= \sigma_0 z + \sigma_1 \frac{dz}{dt} + \sigma_2 \omega_f, \end{aligned} \tag{21}$$

where z is the average deflection of the bristles, ω_f is the velocity between the two surfaces in contact, $g(\omega_f)$ is the

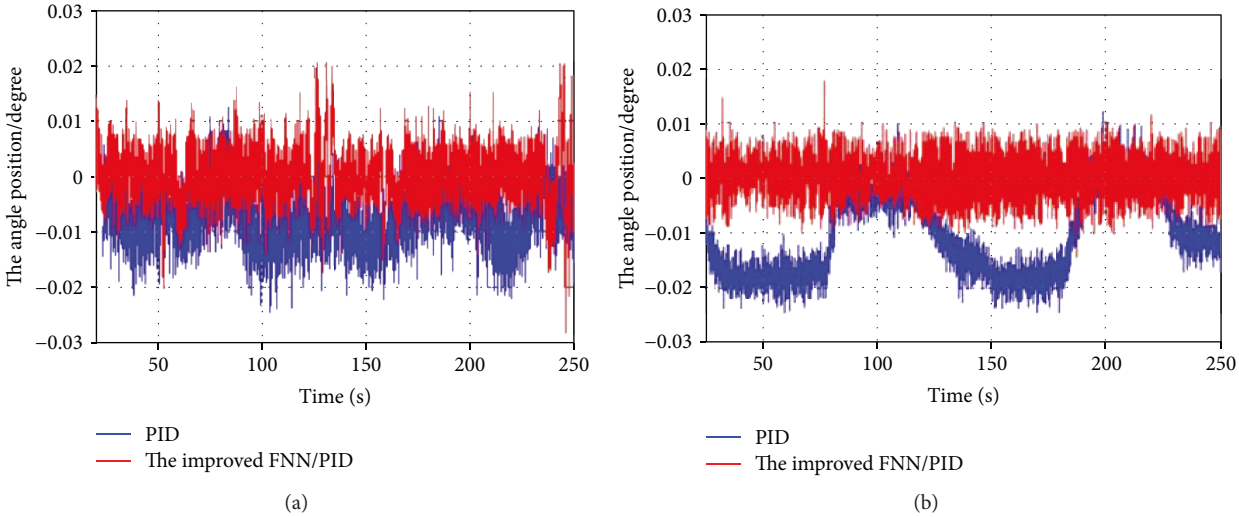

Figure 17: Static levelling experiment results: (a) rolling and (b) pitching.

Table 3: Error comparison of static levelling results.

Frame	RMS errors (°) PID	RMS errors (°) Fuzzy/PID	Improved extent than PID (%)	RMS errors (°) Improved FNN/PID	Improved extent than PID (%)
Rolling	0.0132	0.0065	50.758	0.0055	58.333
Pitching	0.0129	0.0035	72.868	0.0030	76.744

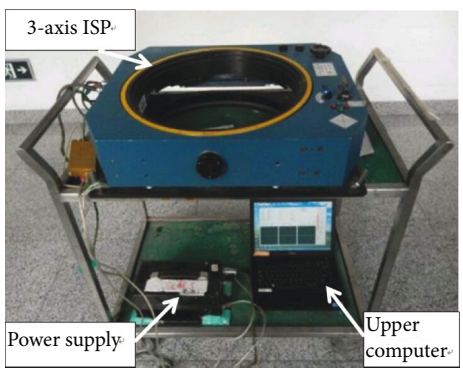

Figure 18: The picture of the three-axis ISP in moving base experiments.

velocity-dependent function, T_c is the coulomb friction torque, T_s is the maximum static friction torque, ω_s is the critical Stribeck speed, σ_0 is the bristle stiffness coefficient of the contact surface, σ_1 is the damping coefficient of the bristles, and σ_2 is the viscous friction coefficient.

4.1. FNN/PID Compound Control Scheme. Figure 10 shows the response curve of the FNN/PID compound control scheme under the step input. As can be seen from this figure, although the angle position errors of the controller determined by the trial and error method can be converged, and the response at the beginning stage is not stable, which has big overshoot errors. However, because of the self-adaptability itself, the controller can achieve the high convergence accuracy eventually.

Table 1 shows the accuracy for the FNN/PID compound control scheme in different periods (root mean square (RMS)). It can be seen that by using the trial and error method, the initial value that makes the system not diverged make the system keep high stabilization accuracy. However, the convergence speed is low and the overshoot is large; meanwhile, since there is an oscillation state in the output process at the early adjustment stage, it is very unfavourable for the work of the motor. In the actual application, it may cause the system to crash in some serious situations. Therefore, it is necessary to optimize the initial values of the parameters in the actual application.

4.2. Improved FNN/PID Compound Control Scheme. As shown in Figure 11, with the step input, the system response curve of the improved FNN/PID compound control scheme has the fast response speed, high stability, and low overshoot. Moreover, the method has a low degree of dependence on the initial value of the weight coefficient.

The RMS errors of the PID, the fuzzy/PID, and the improved FNN/PID compound control scheme are shown in Table 2. The improved FNN/PID compound control scheme has higher accuracy than the previous methods described above. In the table, the RMS errors of the three different methods to the step input are compared at different time stages. We can see that in the whole time stages of 0–30 s, the RMS error of the fuzzy/PID is 0.0770°, which is decreased up to 17.29% than that of the PID, and the

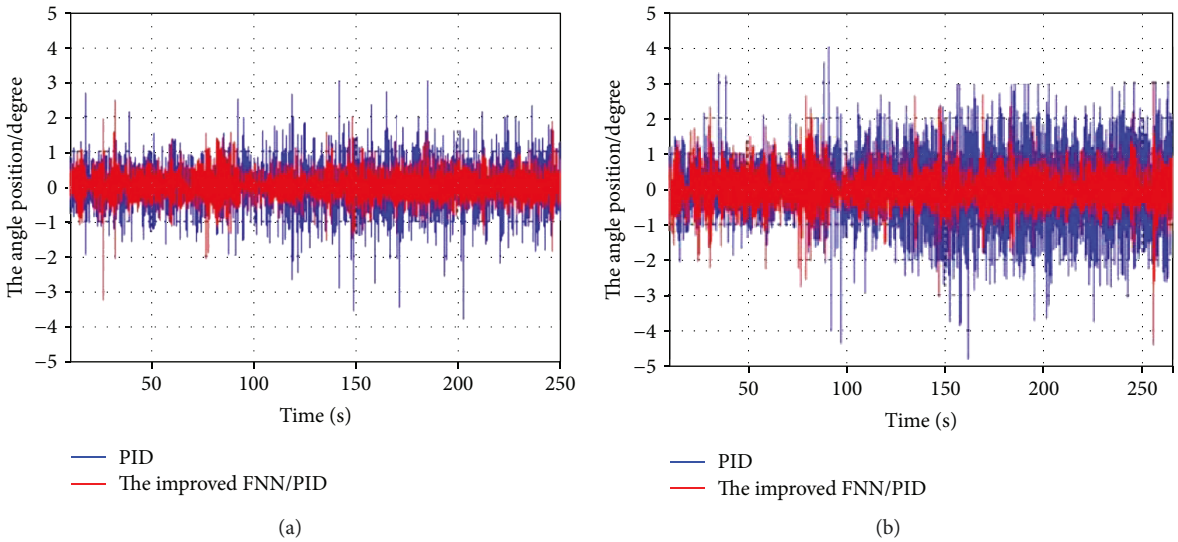

Figure 19: Moving base experiment results: (a) rolling and (b) pitching.

Table 4: Result comparison among three methods under dynamic levelling experiments.

Frame	RMS errors (°) PID	RMS errors (°) Fuzzy/PID	Improved extent than PID (%)	RMS errors (°) Improved FNN/PID	Improved extent than PID (%)
Rolling	0.5942	0.4808	19.084	0.4098	31.033
Pitching	0.9491	0.6590	30.566	0.5493	42.124

RMS error of the improved FNN/PID is 0.0432°, which is decreased up to 53.6% than that of the PID.

Compared with the traditional FNN/PID method, the improved FNN/PID compound control scheme has little dependence on the initial value of the weight coefficient, which has high stability. For the improved FNN/PID compound control scheme with higher stability, the sine signal with an amplitude of 1 and a period of 10 s is input into the system. The sine response curve under the friction disturbance of the system is shown in Figure 12. As can be seen in the figure, compared with the PID (0.0307° RMS error), the RMS error of the improved FNN/PID is decreased up to 99.71%, illustrating its excellent tracking accuracy.

Figure 13 shows the comparison of system responses to sine input among different methods under the friction disturbance. As seen in the figure, three methods are compared with the improved FNN/PID of Figure 12(b), which are the PID, the fuzzy control, and the fuzzy/PID, respectively. Compared with other methods, the improved FNN/PID compound control scheme has better response speed and stabilization accuracy and has a greater ability for disturbance suppression compensation.

5. Experimental Validation

The improved FNN/PID compound control scheme is applied to the actual equipment of the ISP to conduct the static levelling experiment. The hardware is mainly composed of circuit boards, sensors, and actuators. The circuit boards include the main control board, high-precision analog signal acquisition board, motor power driver board, power board, accelerometer signal processing board, and gyro signal processing board, respectively. Among them, the control board with DSP is the core of the entire circuit system, which can realize digital signal processing, high-speed ADC analog-digital conversion, and communication and output motor control PWM signal to the motor power drive unit. The main sensors and actuators include 3 Hall current sensors, 3 rate gyros, 3 photoelectrical encoders, 2 accelerometers, and 3 torqued motors, respectively. The software includes the control software and upper computer software, which are all developed by VC++6.0, as shown in Figures 14 and 15, respectively. The control software is used as the control program of the ISP. The upper computer software is used for monitoring the signal outputs of POS, gyro, and current.

5.1. Static Base Experiments. Figure 16 shows the picture of the three-axis ISP system in levelling static experiments. The weight of the ISP is 40 kg and the weight of the simulated load is 20 kg, and the largest weight that the ISP can carry is 80 kg. The maximum levelling rotation angle range is ±5°; the maximum heading rotation angle range is ±25°.

Figure 17 shows the static levelling experiment results. The stabilization errors (RMS) of the roll and pitch control system are 0.0055° and 0.0030°, which are, respectively, decreased up to 58.333% and 76.744% compared with 0.0132° and 0.0129° of the PID. The comparison results of static levelling are listed in Table 3. We see that the

(a) (b)

Figure 20: Aerial remote sensing system: (a) aerial remote sensing system and (b) integrated remote sensing system in a plane.

Figure 21: High-resolution surveying and mapping maps with a 1 : 500 scale.

stabilization accuracy has been significantly improved, which is in good accordance with the simulation results, illustrating the effectiveness of the improved FNN/PID compound control scheme.

5.2. Moving Base Experiments. Figure 18 shows the picture of the three-axis ISP in moving base experiments. In order to further validate the performance of the proposed method under the movable base, the dynamic experiments are conducted on a movable cart under uneven ground while changing the moving direction. The experimental results are shown in Figure 19. The comparison results among three methods under dynamic levelling experiments are listed in Table 4. It can be known that the stabilization errors (RMS) of the roll and pitch control systems are 0.4098° and 0.5493°, which are, respectively, decreased up to 31.033% and 42.124% than those of the PID, meaning that the disturbance rejection ability of the improved FNN/PID compound control scheme is significant. Figures 20 and 21 show the applications of the ISP in a real aerial remote sensing system, by which the high-resolution surveying and mapping maps with a scale of 1 : 500 were successfully obtained.

6. Conclusions

In this paper, to improve the ability of disturbance rejection and the stabilization accuracy of an aerial ISP, an improved FNN/PID compound control scheme based on variable universe and BP algorithms is proposed. In the compound controller design, the idea of variable universe and the BP algorithm are, respectively, used to improve the capability of the FNN/PID compound control scheme in disturbance rejection and the stabilization accuracy of an aerial ISP. To verify the improved FNN/PID compound control method, the simulations and experiments are carried out, respectively. The results show that the improved FNN/PID compound control scheme has excellent capability in disturbance rejection, by which the ISP stabilization accuracy under dynamic disturbance is improved significantly. Compared to the PID method, the RMS errors of the roll and pitch gimbal systems under the dynamic base obtained by the FNN/PID compound control scheme are decreased up to 31% and 42%, respectively.

Data Availability

The data used to support the findings of this study are available from the corresponding author upon request.

Conflicts of Interest

The authors declare no conflict of interest.

Acknowledgments

This project is supported in part by the National Natural Science Foundation of China (Grant nos. 51775017 and 51375036), by the Beijing Natural Science Foundation (Grant no. 3182021), by the Open Research Fund of the State Key Laboratory for Manufacturing Systems Engineering (sklms2018005). The aerial remote sensing system shown in Figures 20 and 21 is supported by the National High-Tech Research and Development Program of China (Grant no. 2008AA121302) and the National Basic Research Program of China (Grant no. 2009CB724001).

References

[1] J. M. Hilkert, "Inertially stabilized platform technology concepts and principles," *IEEE Control Systems*, vol. 28, no. 1, pp. 26–46, 2008.

[2] X. Zhou, H. Zhang, and R. Yu, "Decoupling control for two-axis inertially stabilized platform based on an inverse system and internal model control," *Mechatronics*, vol. 24, no. 8, pp. 1203–1213, 2014.

[3] J. M. Hilkert and D. A. Hullender, "Adaptive control system techniques applied to inertial stabilization systems," in *Proceedings of SPIE, Acquisition, Tracking, and Pointing IV*, vol. 1304, pp. 190–206, Orlando, FL, USA, September 1990.

[4] P. J. Kennedy and R. L. Kennedy, "Direct versus indirect line of sight (LOS) stabilization," *IEEE Transactions on Control Systems Technology*, vol. 11, no. 1, pp. 3–15, 2003.

[5] X. Zhou, B. Zhao, and W. Liu, "A compound scheme on parameters identification and adaptive compensation of nonlinear friction disturbance for the aerial inertially stabilized platform," *ISA Transactions*, vol. 67, no. 1, pp. 293–305, 2017.

[6] X. Zhou, Y. Jia, and Q. Zhao, "Dual-rate-loop control based on disturbance observer of angular acceleration for a three-axis aerial inertially stabilized platform," *ISA Transactions*, vol. 63, no. 7, pp. 288–298, 2016.

[7] M. K. Masten, "Inertially stabilized platforms for optical imaging systems," *IEEE Control Systems*, vol. 28, no. 1, pp. 47–64, 2008.

[8] X. Lei, Y. Zou, and F. Dong, "A composite control method based on the adaptive RBFNN feedback control and the ESO for two-axis inertially stabilized platforms," *ISA Transactions*, vol. 59, no. 4, pp. 424–433, 2015.

[9] J. Fang, R. Yin, and X. Lei, "An adaptive decoupling control for three-axis gyro stabilized platform based on neural networks," *Mechatronics*, vol. 27, no. 4, pp. 38–46, 2015.

[10] X. Zhou, Y. Jia, Q. Zhao, and R. Yu, "Experimental validation of a compound control scheme for a two-axis inertially stabilized platform with multi-sensors in an unmanned helicopter-based airborne power line inspection system," *Sensors*, vol. 16, no. 3, p. 366, 2016.

[11] H. G. Wang and T. C. Williams, "Strategic inertial navigation systems - high-accuracy inertially stabilized platforms for hostile environments," *IEEE Control Systems*, vol. 28, no. 1, pp. 65–85, 2008.

[12] Z. Lin, K. Liu, and L. Zhang, "Coupling effect and control strategies of the maglev dual-stage inertially stabilization system based on frequency-domain analysis," *ISA Transactions*, vol. 64, no. 4, pp. 98–112, 2016.

[13] X. Zhou, C. Yang, B. Zhao, L. Zhao, and Z. Zhu, "A high-precision control scheme based on active disturbance rejection control for a three-axis inertially stabilized platform for aerial remote sensing applications," *Journal of Sensors*, vol. 2018, Article ID 7295852, 9 pages, 2018.

[14] X. Zhou, C. Yang, and T. Cai, "A model reference adaptive control/PID command scheme on disturbance rejection for an aerial inertially stabilized platform," *Journal of Sensors*, vol. 2016, Article ID 7964727, 11 pages, 2016.

[15] H. Nasser, E. H. Kiefer-Kamal, and H. Hu, "Active vibration damping of composite structures using a nonlinear fuzzy controller," *Composite Structures*, vol. 94, no. 4, pp. 1385–1390, 2012.

[16] P. Li and F. Jin, "Adaptive fuzzy control for unknown nonlinear systems with perturbed dead-zone inputs," *Acta Automation Sinica*, vol. 36, no. 4, pp. 573–579, 2009.

[17] M. Marinaki, Y. Marinakis, and G. E. Stavroulakis, "Fuzzy control optimized by PSO for vibration suppression of beams," *Control Engineering Practice*, vol. 18, no. 6, pp. 618–629, 2010.

[18] D. Wang, X. Lin, and Y. Zhang, "Fuzzy logic control for a parallel hybrid hydraulic excavator using genetic algorithm," *Automation in Construction*, vol. 20, no. 5, pp. 581–587, 2011.

[19] R.-E. Precup, M.-B. Rădac, M. L. Tomescu, E. M. Petriu, and S. Preitl, "Stable and convergent iterative feedback tuning of fuzzy controllers for discrete-time SISO systems," *Expert Systems with Applications*, vol. 40, no. 1, pp. 188–199, 2013.

[20] S. Tong and G. Liu, "Real-time simplified variable domain fuzzy control of PEM fuel cell flow systems," *European Journal of Control*, vol. 14, no. 3, pp. 223–233, 2008.

[21] J. N. Lygouras, P. N. Botsaris, and J. Vourvoulakis, "Fuzzy logic controller implementation for a solar air-conditioning system," *Applied Energy*, vol. 84, no. 12, pp. 1305–1318, 2007.

[22] U. Zuperl, F. Cus, and M. Milfelner, "Fuzzy control strategy for an adaptive force control in end-milling," *Journal of Materials Processing Technology*, vol. 164-165, no. 2, pp. 1472–1478, 2005.

[23] L. A. Zadeh, "Fuzzy sets," *Information and Control*, vol. 8, no. 3, pp. 338–353, 1965.

[24] C. Radu and R. Wilkerson, "Using fuzzy set theory," *IEEE Potentials*, vol. 14, no. 5, pp. 33–35, 1995.

[25] Y. M. Li, Y. B. Wang, and Q. F. Yan, "The technology study of fuzzy control system for asynchronous motor," in *2013 3rd International Conference on Consumer Electronics, Communications and Networks*, pp. 710–713, Xianning, China, November 2013.

[26] J. Zhang, S. Zhang, and Z. Dan, "Variable universe fuzzy PID control for multi-level gas tank pressure," in *2014 IEEE 17th International Conference on Computational Science and Engineering*, pp. 1900–1904, Chengdu, China, December 2014.

[27] S. Xu, Y. Jing, and X. Chen, "Design of fuzzy-CMAC neural-network complex controller for gas mixing process," in *2011 Second International Conference on Mechanic Automation and Control Engineering*, pp. 1191–1194, Hohhot, China, July 2011.

[28] V. N. A. L. Dasilva and R. S. Zubulum, "An integration of neural networks and fuzzy logic for power systems diagnosis," in *Proceedings of International Conference on Intelligent System Application to Power Systems*, pp. 237–241, Orlando, FL, USA, February 1996.

[29] M. Michele and M. Giuseppe, "A gimbal platform stabilization for topographic applications," in *ICNAAM-2014: International Conference on Numerical Analysis and Applied Mathematics 2014*, vol. 1648, pp. 780011-1–780011-4, Rhodes, Greece, September 2014.

[30] W. Pedrycz and M. H. Smith, "Fuzzy inference networks: an introduction," in *Proceedings of International Conference on Neural Networks (ICNN'97)*, pp. 2342–2346, Houston, TX, USA, June 1997.

[31] Y. Cui, X. Li, and Z. Liu, "Application of improved BP neural network with correlation rules in network intrusion detection," *International Journal of Security and its Applications*, vol. 10, no. 4, pp. 423–430, 2016.

[32] T. Kang, J. Fang, and W. Wang, "In-flight calibration approach based on quaternion optimization for POS used in airborne remote sensing," *IEEE Transactions on Instrumentation and Measurement*, vol. 62, no. 11, pp. 2882–2889, 2013.

[33] H. Yang, D. Dong, and Y. Ren, "Study on fuzzy PID control in double closed-loop DC speed regulation system," in *2011 Third International Conference on Measuring Technology and*

Mechatronics Automation, pp. 465–469, Shangshai, China, January 2011.

[34] X. Zhou, L. Li, and Y. Jia, "Adaptive fuzzy/proportion integration differentiation (PID) compound control for unbalance torque disturbance rejection of aerial inertially stabilized platform," *International Journal of Advanced Robotic Systems*, vol. 13, no. 5, 2016.

[35] J. Cervantes, W. Yu, and S. Salazar, "Takagi–Sugeno dynamic neuro-fuzzy controller of uncertain nonlinear systems," *IEEE Transactions on Fuzzy Systems*, vol. 25, no. 6, pp. 1601–1615, 2016.

[36] S. Kara, S. Dasb, and P. K. Ghoshb, "Applications of neuro fuzzy systems: a brief review and future outline," *Applied Soft Computing*, vol. 15, no. 1, pp. 243–259, 2014.

[37] W. Wang, X. Huang, and W. Huang, "Design and simulation of heat substation controller based on neural network-fuzzy PID control," in *2011 Third International Conference on Intelligent Human-Machine Systems and Cybernetics*, pp. 3–6, Zhejiang, China, August 2011.

[38] J. Li and J. Yu, "An intelligent control system based on recurrent neural fuzzy network and its application to CSTR," *Journal of Systems Science and Complexity*, vol. 18, no. 1, pp. 43–54, 2005.

[39] X. Zhou, G. Gong, J. Li, H. Zhang, and R. Yu, "Decoupling control for a three-axis inertially stabilized platform used for aerial remote sensing," *Transactions of the Institute of Measurement and Control*, vol. 37, no. 9, pp. 1135–1145, 2015.